Geologic Map of the Rochester 7.5-minute Quadrangle, Thurston and Lewis Counties, Washington

Michael Polenz[1], Conner H. Toth[1], Catherine Samson[1], Andrew J. Sadowski[1], Rebeca I. Becerra[1], Todd R. Lau[1], Megan L. Anderson[1], Elizabeth A. Nesbitt[2], Jeffrey H. Tepper[3], S. Andrew DuFrane[4], and Gabriel Legorreta Paulín[5]

[1] Washington Geological Survey, [2] The Burke Museum of Natural History and Culture, University of Washington, [3] Geology Department, University of Puget Sound, [4] University of Alberta Department of Earth and Atmospheric Sciences, [5] Instituto de Geografía Universidad Nacional Autónoma de México Ciudad Universitaria

November 2019

WASHINGTON STATE DEPARTMENT OF NATURAL RESOURCES
WASHINGTON GEOLOGICAL SURVEY

WASHINGTON GEOLOGICAL SURVEY
MAP SERIES 2019-02
Geologic Map of the Rochester 7.5-minute Quadrangle

©2019 Washington Geological Survey
http://www.dnr.wa.gov/geology

State of Washington Licensed Geologist 705 POLENZ, MICHAEL
Michael Polenz
November 2019

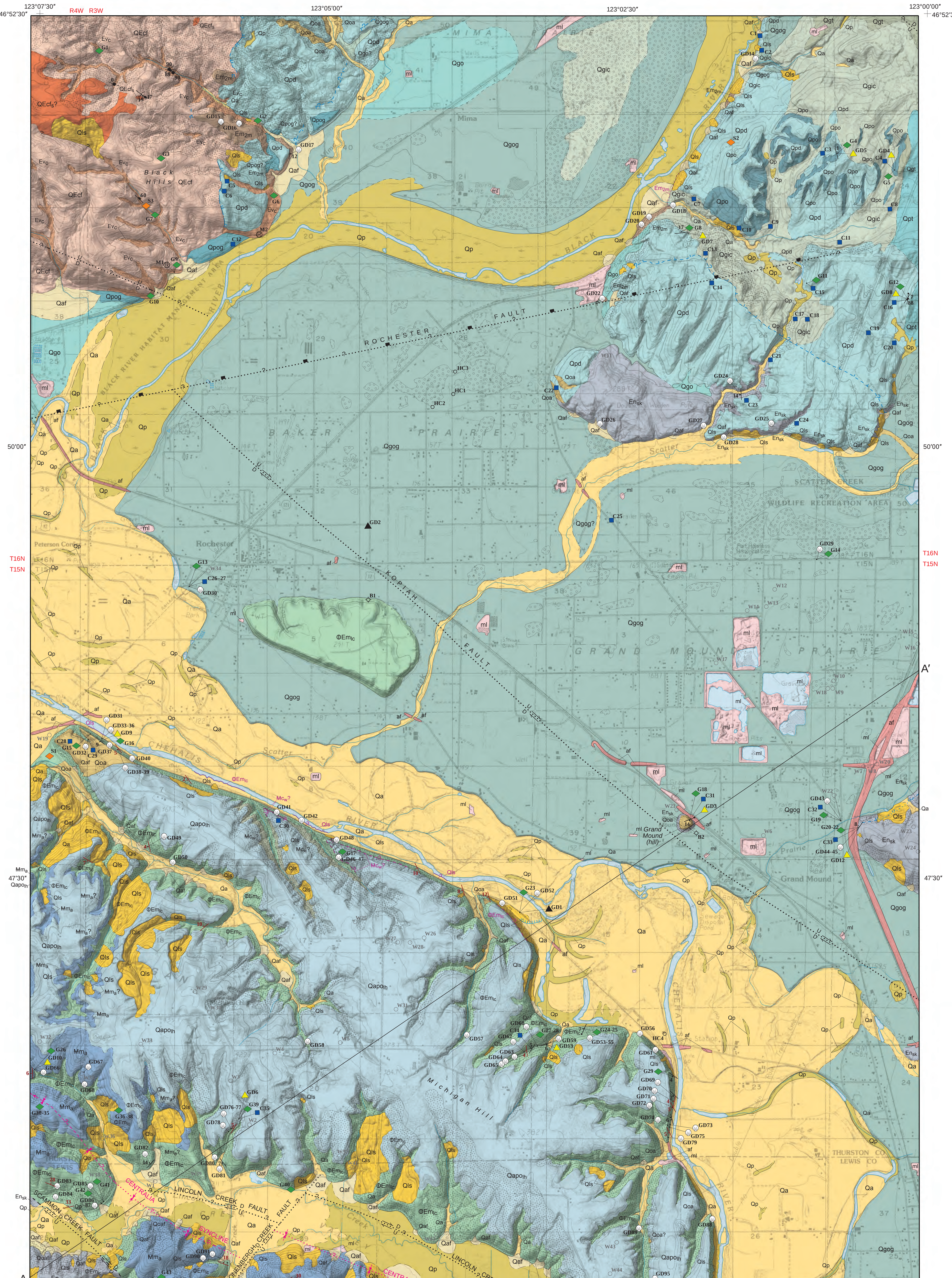

ABSTRACT

The Rochester quadrangle straddles Thurston and Lewis Counties west of Washington's economically vital I-5 freeway. This map supports private and public resource management and planning with insights into geologic deposits, structures, and hazards. Field- and lidar-informed mapping improve identification of landslides and Mima mounds, confirming that the latter occur only on outwash. Vashon Drift and deposits from at least one earlier Cordilleran ice incursion reached their southern limit in the quadrangle. Outwash provides ample gravel resources and a productive aquifer. New detrital zircon U-Pb ages provide maximum depositional ages for: (1) the Lincoln Creek Formation type section near Galvin (<28.6 ±2.1 Ma) and Helsing Junction (<20.3 ±1.7 Ma), confirming that the formation ranges into the Miocene; (2) the Astoria(?) Formation south of Helsing Junction (<22.1 ±1.5 Ma), suggesting that its age may overlap with that of the Lincoln Creek Formation; (3) the Logan Hill Formation on Michigan Hill (<1.9 ±0.8 Ma), where a lack of Miocene zircons suggests that sedimentary provenance differs from Logan Hill Formation farther south; (4) strongly weathered drift from northern-sourced, pre-Vashon ice incursion(s) (<2.4 ±1.6 Ma; <3.0 ±0.7 Ma; <0.8 ±1.0 Ma; <1.4 ±0.2 Ma); and (5) a relict terrace on Grand Mound (unit Qoa, <0.3 ±0.5 Ma), which implies about 100 ft of net valley-floor lowering during the last approximately 0.7 Ma. New geochemical data suggest that volcaniclastic rocks in the Astoria(?) Formation are derived from the volcanic rocks of Grays River. Faults in the map area are interpreted in the context of regional north–south compression.

GEOLOGIC OVERVIEW

This map revises and refines prior, smaller-scale mapping (Snavely and others, 1958; Wallace and Molenaar, 1961; Weigle and Foxworthy, 1962; Noble and Wallace, 1966; Logan, 1987; Walsh and others, 1987). The oldest rocks in the map area are lower Eocene Crescent Formation basalt of the Siletzia terrane (Wells and others, 2014), located in the Black Hills near the northwest map corner. East and south thereof, deposition of marine, middle Eocene McIntosh Formation onlaps Crescent Formation and was followed, in succession, by deltaic to freshwater deposition of middle to upper Eocene Skookumchuck Formation, an unconformity, and marine deposition of the upper Eocene to Miocene Lincoln Creek and the Miocene Astoria Formations. Late Miocene Wilkes Formation documents a return of deltaic to freshwater conditions. Exposure of these rocks is controlled by the southeast-plunging Centralia syncline (Snavely and others, 1958; Logan, 1987; Walsh and others, 1987) and Rochester Basin, bounded on the north by the north-up Rochester fault, on the northeast by the northeast-up Kopiah fault, and on the southwest by the southwest-up Scammon Creek fault. The Lincoln Creek, Astoria, and Wilkes Formations are exposed within the syncline and basin; the (older) Crescent, McIntosh, and Skookumchuck Formations are exposed north, northeast, and southwest of the syncline and basin. The structures are interpreted below in the regional context of Miocene to present north–south shortening (Johnson and others, 2004; McCaffrey and others, 2013).

Till from at least two incursions of glaciers moving south from the Puget Lowland into the map area conceals most bedrock near the northeastern map corner. Outwash gravel from these ice incursions forms broad prairies across the valleys of the Black River, Scatter Creek, and the Chehalis River. Farther southwest, alpine outwash gravel of the Logan Hill Formation forms a flat cap of deeply weathered soil above the Eocene to Miocene sedimentary rocks.

GEOLOGIC SYMBOLS

Mass-wasting landforms (overlay pattern)—Landforms that suggest mass movement on unstable slopes, but evidence for landslide deposits is inconclusive.

Mima mounds (overlay pattern)—Dark brown to black, organic-rich sand to pebbly sandy loam soil in regularly spaced round to oval mounds about 2 to 6 ft high and 10 to 30 ft across; little or no soil between mounds; black color mostly from burned organic matter. Mounds rest on terraces of highly permeable Vashon proglacial outwash of northern- and Cascade Range-sourced pebbles and cobbles. Mapped where landforms and (or) field-observed deposits indicate the presence of such mounds.

Contact—Solid where location accurate; long-dashed where approximate; short-dashed where inferred

Reverse fault—Identity or existence questionable; location concealed; rectangles on upthrown block

High-angle dip-slip fault—Identity or existence questionable; short-dashed where inferred; dotted where concealed; relative motion shown by U and D

Oblique-slip fault, reverse right-lateral offset—Solid where location accurate; short-dashed where inferred; dotted where concealed; queried where identity or existence questionable; relative horizontal motion shown by arrows, relative vertical motion shown by U and D

Oblique-slip fault, high-angle left-lateral offset—Concealed; queried where identity or existence questionable; relative horizontal motion shown by arrows, relative vertical motion shown by U and D

Syncline—Identity or existence questionable; short-dashed where inferred; dotted where concealed; arrow on line indicates plunge direction

Qgag — Geologic unit too thin to show as a polygon—Solid where location accurate; long-dashed where approximate; short-dashed where inferred; dotted where concealed; queried where identity or existence questionable

Continental ice limit, late Wisconsinan—Identity or existence questionable; inferred

Continental ice limit, pre–late Wisconsinan—Long-dashed where approximate; short-dashed where inferred; dotted where concealed

A —— A′ Cross section line

Perennial stream

Intermittent stream

Fluvial terrace—Location accurate; hachures point down slope

14, 36 Inclined bedding—showing strike and dip; **black symbols** collected by Washington Geological Survey; **red symbols** compiled from Snavely and others (1958)

9 Approximate orientation of inclined bedding in unconsolidated deposits or bedrock—showing approximate strike and dip

Approximate horizontal bedding

14 Inclined bedding, where top of direction of beds is known from local features—showing strike and dip

89 Small, minor inclined joint—showing strike and dip

90 Small, minor vertical or near-vertical joint—showing strike

17 Inclined slickenline, groove, or striation on fault surface—showing bearing and plunge

19 Shear—showing strike and dip

GD88 Age site, fossil

GD6 Age site, U-Pb, uranium-lead

GD1 Age site, ^{14}C, carbon-14

G10 Geochemistry sample location

W22 Water well

S2 Significant site

HC1 Drill hole for hydrocarbon exploration

B3 Drill hole or test pit

M2 Paleomagnetic sample—reverse magnetization

C22 Clast count sample

Lambert conformal conic projection
North American Datum of 1927; to place on North American Datum of 1983, move the projection lines approximately 24 meters north and 97 meters east as shown by crosshair corner tics
Base map from scanned and rectified U.S. Geological Survey Rochester 7.5-minute quadrangle, 1986, revised 1993
Shaded relief generated from a lidar bare-earth digital elevation model (available from the Washington Geological Survey, http://lidarportal.dnr.wa.gov/)
GIS by Michael Polenz, Conner Toth, Rebeca Becerra, and Cat Samson
Digital cartography by Daniel E. Coe
Editing and production by Susan R. Schnur and Maria A. Furtney

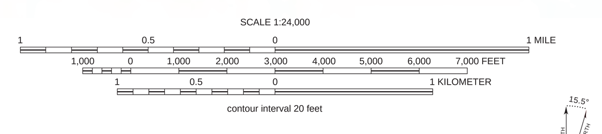

This geologic map was funded in part by the U.S. Geological Survey National Cooperative Geologic Mapping Program under USGS award number G18AC00190, 2018–2019.

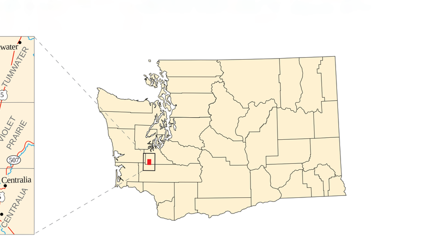

Research supported by the U.S. Geological Survey, National Cooperative Geologic Mapping Program, under USGS award number G18AC00190. The views and conclusions contained in this document are those of the authors and should not be interpreted as necessarily representing the official policies, either expressed or implied, of the U.S. Government.

Disclaimer: This product is provided 'as is' without warranty of any kind, either expressed or implied, including, but not limited to, the implied warranties of merchantability and fitness for a particular use. The Washington Department of Natural Resources and the authors of this product will not be liable to the user of this product for any activity involving the product with respect to the following: (a) lost profits, lost savings, or any other consequential damages; (b) fitness of the product for a particular purpose; or (c) use of the product or results obtained from use of the product. This product is considered to be exempt from the Geologist Licensing Act [RCW 18.220.190 (4)] because it is geological research conducted by or for the State of Washington, Department of Natural Resources, Washington Geological Survey.

CROSS SECTION EXPLANATION

Qp | Qa — Geologic units too thin to show as polygons at the scale of the cross section; vertical tics mark separate units.

Arrows show relative fault movement in the plane of the cross section.

⊗ ⊙ Arrow point shows fault movement toward the viewer; arrow feathers show fault movement away from the viewer.

W7 Water well or boring

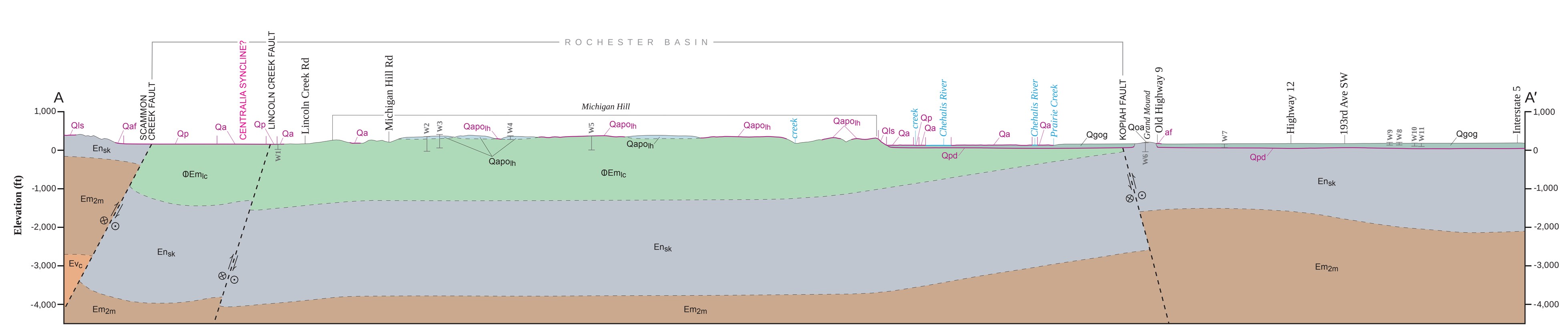

GEOCHEMISTRY

Whole-rock chemical analyses on 16 volcanic rock samples from the Rochester quadrangle include nine clasts from the Astoria(?) Formation and seven bedrock samples.

The bedrock samples are tholeiitic basalts (Figs. M2A, B) of limited compositional diversity (48.4–48.8 wt.% SiO_2, 7.2–9.0 wt.% MgO, molar Mg/Mg+Fe (Mg#) = 0.61–0.52). Both major and trace element data support assignment of these basalts to the Crescent Formation (Table M1; Fig. M2), although the Rochester quadrangle basalts are slightly more primitive than other Crescent Formation rocks averaged in Table M1. This difference is reflected in higher average MgO and Cr contents of the Rochester quadrangle basalts. In the adjacent Littlerock quadrangle, Polenz and others (2017) divided Crescent Formation basalts into a less-enriched group and a more-enriched group on the basis of trace element abundances. The Rochester quadrangle samples have some attributes of both groups. Compositional diversity among Crescent Formation basalts likely reflects variability in mantle source chemistry and extent of differentiation.

The nine clasts from the Astoria(?) Formation are alkaline and range from picrobasalt to trachyandesite (Fig. M2A). The basaltic samples are compositionally diverse (for example, 2.1–10.5 wt.% MgO, 0.56–1.69 wt.% K_2O, 10–380 ppm Cr), but all of the clasts, including the trachyandesite, are characterized by light rare earth element enrichment (La/YbN = 10.3–22.4), high levels of incompatible trace elements (for example, 44–110 ppm Nb, 210–1000 ppm Zr), and low Ba/Nb (6.3–8.2). Incompatible element abundances are inversely correlated with MgO, suggesting that much of the compositional diversity resulted from fractional crystallization. The low Ba/Nb, high TiO_2, and absence of Ta-Nb depletions on a spidergram (Fig. M2D) preclude derivation of the Astoria(?) clasts from a Cascade Arc source or a Columbia River Basalt flow. However, the clasts share many chemical traits with the volcanic rocks of Grays River (GRV) (Phillips and others, 1989; Chan and others, 2012)(Table 1; Figs. M2C–D). Some differences between the clasts and the GRV (lower SiO_2, higher Fe_2O_3T) could be due to weathering, but the higher levels of immobile trace elements (such as Nb, Zr) and higher La/YbN are almost certainly primary igneous traits. The Astoria(?) Formation clasts were likely derived either from GRV flows that are more enriched than those sampled by Chan and others (2012), or from another forearc volcanic unit, that may no longer exist.

GEOPHYSICS

An isostatic gravity map was built from new gravity stations at 1–2 km grid spacing with lines across features of interest at 250 m spacing (Lau and others, 2018). We applied a horizontal gradient filter to the isostatic gravity grid and used an algorithm to select linear maxima ("max spots"). Recent aeromagnetic data (Blakely and others, 2016), new ground magnetic data, and 151 new rock density measurements also support our interpretations. The Black Hills and Lincoln Creek uplifts (BH and LCU in Fig. M1) are gravity highs due to near-surface basaltic basement. Gravity lows result from thick low-density sediments above the basalt. The Rochester Basin (RB in Fig. M1) is a gently southeast-plunging gravity low northeast of the Lincoln Creek uplift and is bounded by the Rochester, Kopiah, and Scammon Creek faults and their associated gravity gradients (RF, KF, and SCF in Fig. M1).

STRUCTURES

The map area lies within the forearc of the seismically active Cascadia subduction zone. We interpret the structures in the map area as potentially active in the context of Miocene to present north–south compression within the forearc (Johnson and others, 2004; McCaffrey and others, 2013; Wells and McCaffrey, 2013), consistent with recent mapping nearby (Polenz and others, 2017, 2018; Sadowski and others, 2018, 2019; Anderson and others, 2018). Pleistocene structural activity is specifically suggested by a gentle, 10-ft-high downstream rise of the unnamed valley at significant site S1, near Helsing Junction (Fig. M1). Field evidence suggests that the elevated downstream end of the valley floor lacks alluvial deposits. Uplift of that valley segment relative to farther upstream could explain such a fluvial-morphologic anomaly. A Pleistocene or younger age can be inferred because deformation of the valley floor must post-date incision of the valley, and 0.3 ±0.5 Ma relict alluvium at GD3 (100 ft above the modern Chehalis River valley floor at Grand Mound), suggests that the valley floor at S1 was incised less than 0.72 million years ago.

Within and near the map area, a fabric of northwest-trending aeromagnetic anomalies (fig. M2 of Polenz and others, 2018) and topographic lineaments parallels the Kopiah and Scammon Creek faults (Snavely and others, 1958; Polenz and others, 2018; Sadowski and others, 2018, 2019). Farther north in the Puget Lowland, detailed study of a similar fabric of aeromagnetic anomalies and topographic lineaments led Sherrod and others (2008) to recognize a broad zone of deformation riddled with fault strands. A similar pattern in the Rochester quadrangle likewise suggests the presence of many unmapped, additional faults in the map area. Three questioned faults aligned with this fabric are shown near the northern map edge.

FAULTS

Scammon Creek fault

The southeast-striking Scammon Creek fault (Snavely and others, 1958) crosses the southwest corner of the map. The fault alignment shown is a synthesis of field observations and combined modeling of gravity and magnetic anomalies. Exposure of Eocene rocks southwest of the fault and younger rocks northeast of it suggests relative southwest-up offset. Reverse offset on a 75° southwest-dipping fault plane was documented in a trench about 3.2 mi west of the map area (Fig. M1), where Washington Public Power Supply System (1974) concluded that the fault has not moved in at least 83,000 years. Several northwest-trending scarps and lineaments near the mapped fault may be either topographic expressions of bedding planes or unmapped fault strands. A singular, steep, northwest-trending gravity gradient (SCF in Fig. M1) splits into two gradients near a left step of the fault at the southern map edge, suggesting the fault may bifurcate there. This is consistent with transpression.

Lincoln Creek fault

The Lincoln Creek fault is newly inferred from modeling of gravity (LCF in Fig. M1) and magnetic anomalies south of the map area (fig. M2 in Polenz and others, 2018) and along Cross Section A–A′. The anomalies are subdued in the map area but strengthen southeastward, especially south of the map area, where Sadowski and others (2019) estimate 1,500 ft of slip. If coeval with the Scammon Creek fault in a north-south-compressional stress field, then the fault would be southwest-dipping, oblique right-lateral reverse—here interpreted as a probable splay in a left step of the Scammon Creek fault.

Sponenbergh Creek fault

The Sponenbergh Creek fault, near the southwest map corner, was mapped but not named by Snavely and others (1958). We name the fault for ease of reference but shorten its trace due to lack of data at its northeast end. Southeast-up offset on the northeast-striking fault is inferred from the juxtaposition of Skookumchuck Formation at the southern map edge against 400 ft of Lincoln Creek Formation in boring B3, immediately northwest of the fault (Snavely and others, 1958). Left-lateral offset is suggested by (1) Snavely and others' (1958) mapping of a left step of the Scammon Creek fault where that fault is cut by the Sponenbergh Creek fault; (2) the distribution of adjacent map units; and (3) an apparent geomorphic left step of Lincoln Creek Valley. High-angle left-lateral oblique-slip and a southeast-dipping fault plane are inferred if the fault exists in a north-south compressional stress field.

Kopiah fault

Exposures of lower Skookumchuck Formation northeast of the northwest-striking Kopiah fault and (younger) Lincoln Creek Formation southwest of the fault support northeast-up offset within and east of the map area (Snavely and others, 1958; Walsh and others, 1987; Polenz and others, 2018; Sadowski and others, 2018). The inference is strengthened by Lincoln Creek Formation, southwest of the fault, extending to depths of 400 ft below the surface in a USGS test boring (B1) and 800 ft in a Pacific States Oil Co. well (HC4) (Snavely and others, 1958). Snavely and others (1958) and Polenz and others (2018) further documented a bedding dip change from mostly gentle with variable strikes in Skookumchuck Formation northeast of the fault to systematically southwest-dipping Lincoln Creek Formation southwest of it, as well as steepening near the fault. Evidence for north–south compression along the fault southeast of the map area (Sadowski and others, 2018) suggests a northeasterly fault dip in the map area. A subtle gravity gradient coincides with the fault (KF in Fig. M1), and lower gravity southwest of this gradient indicates relative northeast-up offset. We show the Kopiah fault terminating at the Rochester fault because the gravity gradient associated with the Kopiah fault ends there. Magnetic data (fig. M2 in Polenz and others, 2018) suggest a similar pattern.

Rochester fault

The existence of the concealed Rochester fault is supported by steep and pronounced north-up gravity and magnetic anomalies (Bromery, 1962; Washington Public Power Supply System, 1974). An east-northeast-trending, steep gravity gradient (RF in Fig. M1) marks the boundary between high gravity in the Black Hills uplift and low gravity in the Rochester basin. This contrast requires basaltic bedrock south of the Black Hills to drop to a greater depth beneath the Chehalis River valley than can be explained by erosion (Lau and others, 2018). The anomaly's linearity, magnitude, and similarity of the anomaly in orientation to the Doty fault (Fig. M1) suggest a steeply dipping fault with substantial north-up offset. Fault offset also explains exposures of McIntosh Formation north of the fault, in contrast to 1,700 ft of Skookumchuck Formation at HC3 south of the fault (Rau, WGS, unpub. records, 1963). Importantly, maximum surface elevations in the glaciated low hills around the east end of the fault are slightly greater north of the fault than south of it. In a north–south compressional stress field, the fault would dip north near the southern margin of the anomalies, as shown.

FOLDS

The southeast-trending Centralia syncline of Snavely and others (1958) is broadly expressed in the Rochester quadrangle as a fault-bounded, downthrown block (Rochester basin in Cross Section A–A′) that crosses the center of the map and extends beyond the map boundaries. A gravity trough (Fig. M1) and the spatial distribution of map units define the basin, with younger units in the basin flanked by Eocene rocks outside it. Bedding data within the basin locally suggest the Centralia syncline as an asymmetric, gently north-west-plunging fold near the southwest map corner (modified from Snavely and others, 1958), but the northwest plunge contrasts with southeast-deepening of the larger Rochester basin gravity trough and southeast-deepening of the contact between the Lincoln Creek and Skookumchuck Formations between B1 and HC4. The Centralia syncline as mapped within the quadrangle therefore is a relatively small feature within the broader, southeast-deepening Rochester basin.

CORRELATION OF MAP UNITS

PERIODS AND EPOCHS BASED ON USGS FACT SHEET 2010-3059

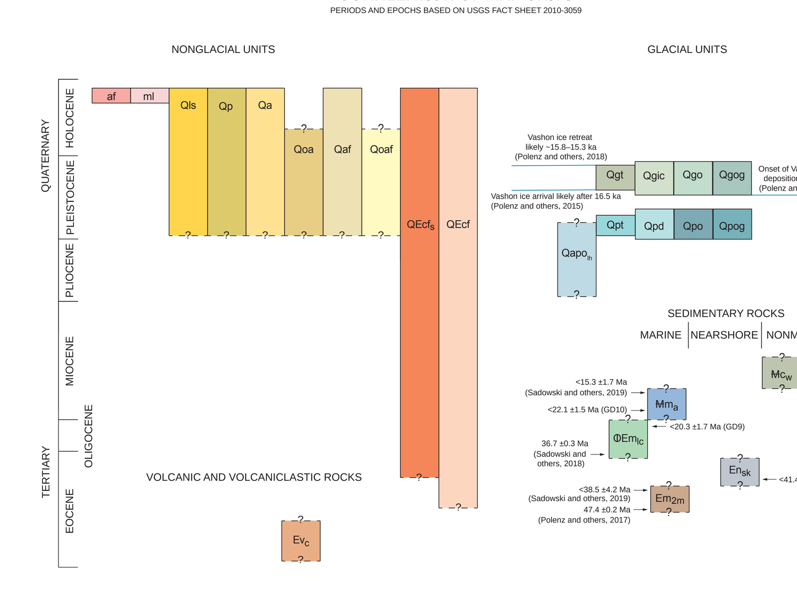

DESCRIPTION OF MAP UNITS

Quaternary

HOLOCENE TO PLEISTOCENE NONGLACIAL DEPOSITS

af — **Artificial fill**—Cobbles, pebbles, sand, silt, clay, and boulders, in various amounts, engineered and non-engineered; used to raise roadbeds and other surfaces. Excludes small or shallow fills (less than 5 ft deep) such as most road-related fills.

ml — **Modified land**—Locally derived soil, cobbles, pebbles, sand, silt, clay, and boulders, in various amounts, reworked by excavation and (or) redistributed to modify topography; includes gravel pits and other developments. Excludes small or shallow reworking such as most road-related modifications with less than 5-ft-deep deposits.

Qls — **Landslide deposits**—Sand, silt, clay, cobbles, pebbles, and boulders, in various amounts, derived from units upslope; varied weathering; clasts angular to rounded; typically loose and unsorted; locally stratified in blocks; primarily mapped from landforms expressed in lidar; mainly found in the unglaciated, sediment-covered hills southwest of the Chehalis River. Streamside landslides along the northeast side of Michigan Hill document cliff collapses that likely dammed the Chehalis River. At GD1 a landslide is queried because a bouldery diamicton tentatively interpreted as a slide mass could instead be railroad fill. A log buried between the diamicton and underlying floodplain sand (unit Qa) yielded a 150 ±30 ^{14}C yr. B.P. maximum depositional age (GD1, Table M2, Table DS1A), which is too young to rule out historic fill.

Qp — **Peat**—Peat, gyttja, muck, silt, clay, and sand in wetland areas and other flat-bottomed depressions, commonly crescent-shaped in relict alluvial channels. Larger peat areas flank Lincoln Creek and the Black River and likely developed when outwash deposition raised the Chehalis River valley floor.

Qa, Qoa — **Alluvium**—Pebbles, cobbles, sand, silt, clay, peat, and boulders in varied amounts along stream channels and floodplains; gray to pale gray and brown to pale brown; fresh to mildly weathered except where addition of proximally derived, weathered particles locally led to bimodal weathering; loose; mostly well rounded and moderately to well sorted; lithologically varied. Unit Qa is widespread along the Chehalis River, Lincoln Creek, and Scatter Creek. Unit Qoa is mapped where active channels no longer contribute to the deposit.

Qaf, Qoaf — **Alluvial fan**—Silt, sand, and gravel in broad, concentric lobes at the confluence of steeper, narrow drainages and a flatter valley floor; gray to brown; loose; subangular to rounded; moderately to poorly sorted; stratified to unstratified. Mostly mapped from landforms expressed in lidar. Unit Qoaf is mapped where streams no longer move sediment onto the surface.

PLEISTOCENE TO PLIOCENE GLACIAL SEDIMENTS

Continental drift

Ice from the Puget lobe of the Cordilleran ice sheet entered the map area from the north during the late Wisconsinan Vashon Stade (marine oxygen isotope stage 2) and one or more earlier glaciations. Deposits from these ice advances (hereafter "northern-sourced" drift) largely resemble each other in lithology and structure, but more advanced and more varied weathering separates the older drift from Vashon Drift—except where waterlogging or burial impeded weathering, as is suggested by clast counts from some well cuttings (C27 and C32 from wells W34 and W22).

Near its southern terminus, the Vashon-age Puget ice lobe was divided into a western (Olympia) and eastern (Yelm) lobe (Bretz, 1913; Walsh and Logan, 2005). Clast assemblages associated with the Olympia lobe contain 30–60% basalt and 15–35% intermediate igneous and granitoid rocks, 5–25% quartz and chert, and 2–13% metamorphic rocks; clast assemblages associated with the Yelm lobe tend to contain more intermediate igneous rocks (22–46%) at the expense of quartz, chert, basalt, and metamorphic rocks (Table DS3). Pre-Vashon drift lithologies are similar (Table DS3) and consistent with trends documented in nearby areas (Polenz and others, 2017, 2018), and we infer pre-Vashon Olympia and Yelm ice lobe(s). A detrital zircon U-Pb age spectrum from Vashon Drift in Olympia (Steely, WGS. unpub. data, 2019) resembles four spectra from earlier drift(s) in the map area (Tables DS1C, GD4; DS1D, GD5; DS1F, GD7; DS1G, GD8) suggesting similar sediment sources. Till in the map area is from the Olympia lobe; outwash includes Olympia and Yelm lobe assemblages.

The location of the map area at the southern ice limit suggests that glaciers entered the map area only during the strongest global glaciations. A strengthening of glacial maxima starting roughly 1 Ma (Pena and Goldstein, 2014) therefore suggests that the pre-Vashon drift(s) in the map area are <1 Ma old. Maximum depositional ages of the youngest zircons from four pre-Vashon drift samples are consistent with this age range (GD4 and GD5, unit Qpo, and GD7 and GD8, unit Qpd; Table M2 and Table DS1A). Weathering of pre-Vashon drift is mostly strong but varies widely (Table DS3) and suggests that these deposits could be from more than one ice advance.

For timing of the Vashon ice advance into the map area, we refer to Polenz and others' (2015) fig. 3 and discussion and suggest that the glacial limit extended south to the Rochester quadrangle.

Qgog — **Vashon recessional outwash gravel**—Pebbles and cobbles, well sorted and clast-supported locally with matrix and interbeds of silt and sand; gray to pale gray, or mildly weathered to pale brown, brown, or variegated with iron stains; almost everywhere loose, but locally lightly cemented; well rounded to subrounded; moderately to well sorted; faintly bedded or unbedded; northern sourced, variously from the Olympia and Yelm ice lobes. Well records typically indicate 60–100 ft thickness. Unit Qgog forms flat to gently undulating surfaces in Baker, Grand Mound, and Mima Prairies, widely dotted with enigmatic Mima mounds (Bretz, 1913; Washburn, 1988; Logan and Walsh, 2009; Burnham and Johnson, 2012; Gabet and others, 2016). Unit Qgog is excessively drained and thus prone to drought. Age site GD2 (Table M1, DS1A) is from 50 ft depth in a well and if not contaminated suggests either that modern roots reach down to 50 ft below the surface or that groundwater flushes root fragments down to the bottom of the vadose zone at that depth. Unit Qgog and its older equivalent (unit Qpog) form a productive aquifer that is sensitive to pollution (Polenz and others, 2018).

Qgo — **Vashon recessional outwash, undivided**—Pebbles, cobbles, sand, and silt, in varied amounts; pale gray, weathers orange or reddish brown; mildly weathered; loose but may be mildly cemented locally; well rounded and moderately or well sorted in most exposures; bedding cross-stratified to unbedded, with channel barforms and channel scour; locally planar bedded in sand and silt; northern-sourced, mostly from the Olympia ice lobe. Between the Black Hills and unit Qgog, unit Qgo consists entirely of silt and fine sand (and may include post-glacial alluvium in the western part of this area). This fine-grained facies may be an inner channel bend slackwater deposit and, unlike coarser outwash surfaces, appears to lack Mima mounds.

Qgic — **Vashon ice contact deposits**—Undivided till and outwash, consisting of loose to compact diamicton, pebble gravel (locally cobbly) and sand; pale gray to brown and reddish brown; mildly weathered; mostly loose and crumbly in ablation till and outwash, ranging to compact in lodgment till; particle size ranges from cobbles to medium sand, with finer particles in till matrix and coarser clasts locally in till; varied rounding and sorting; northern sourced, mostly from the Olympia ice lobe but clast lithologies in some outwash deposits suggest derivation from the Yelm lobe. Unit thickness is highly varied; much of the unit is likely less than 10 ft thick, but geomorphic field relations suggest more than 50 ft locally. Unit Qgic includes the Vashon-age southern terminal moraine and is marked by irregular landforms such as eskers, kettles, and drumlin and flute surfaces that are usually rougher than those in unit Qgt.

Qgt — **Vashon lodgment till**—Diamicton containing boulders to sand with a matrix ranging from sand to clay, in various amounts; gray to pale, reddish brown; mildly to moderately weathered; mostly compact to very compact; clasts angular to well rounded; unsorted and nearly everywhere matrix supported; northern sourced from the Olympia ice lobe. Unit Qgt is mostly inferred along the northern map boundary based on landforms and adjacent mapping. It was also observed about one mile farther south near U-Pb age site GD4. Compact till locally observed elsewhere is included in unit Qgic.

Qpt — **Pre-Vashon till**—Diamicton, containing boulders to sand with a matrix mostly of clay; light brown to red, orange, and pale yellow; matrix and clasts are distinctly weathered, with mostly secondary clay in the matrix; compact but in most exposures too weathered to retain compaction; clasts subangular to subrounded; unsorted and unstratified; northern sourced from the pre-Vashon Olympia ice lobe. Pre-Vashon till is mapped along the east edge of the map area within two miles of the northern map edge. It is widespread elsewhere in the northeastern hills of the map area but is included in undivided drift unit Qpd because most exposures are either very localized or too weathered to recognize separately from ablation till or outwash.

Qpog — **Pre-Vashon outwash gravel**—Pebbles and cobbles, with sparse to moderately voluminous sandy to clayey matrix; pale gray; weathers pale brown to tan and light orange; moderately to strongly weathered, locally mildly weathered, especially below the water table (such as at clast count samples C27 (W34) and C32 (W22); Table DS3); loose to moderately compact; moderately to well sorted; rounded to subangular; northern sourced, variously from the Olympia and Yelm ice lobes. Unit Qpog is exposed in terraces along the southeastern base of the Black Hills. Based on well records, the unit is inferred at depth beneath Mima, Baker, and Grand Mound Prairies, and constitutes most of unit Qpd in Cross Section A–A′. Some of the terrace exposures along the Black Hills were previously mapped as Vashon outwash (Snavely and others, 1958; Logan, 1987) but are here mapped as unit Qpog based on weathering. Clast weathering at C12 closely resembles Possession-age sample C42 of Polenz and others (2017) 2.7 mi north of the Rochester quadrangle. Their sample C51 is more strongly weathered than their sample C42 from the same location and indicates that some of the more weathered outwash in the map area may also be Possession-age.

Qpo — **Pre-Vashon outwash, undivided**—Cobbles, pebbles, sand, silt, and clay, in varied amounts; pale yellowish brown to orange, reddish brown and variegated; moderately weathered to rotten; moderately to strongly compacted; sand is fine- to medium-grained where not weathered to clay; subangular to well rounded; mostly well sorted; mostly stratified; northern sourced, from the Olympia and Yelm ice lobes. Some exposures are easily confused with weathered bedrock (for instance, at GD4). Unit Qpo is locally capped by patchy and weathered diamicton that is till in some exposures but elsewhere may be a product of soil development in outwash of unit Qpo. Unit Qpo is locally exposed in the glaciated northeastern hills of the map area but also forms part of the undivided pre-Vashon drift inferred from well records and drill core samples beneath Mima, Baker, and Grand Mound prairies.

Qpd — **Pre-Vashon drift, undivided**—Diamicton, pebbles, cobbles, sand, silt and clay, in varied amounts; light orange to brown, yellowish brown, red, olive-green, gray or variegated; mostly compact, with some exposures resembling mildly indurated, strongly weathered bedrock, but in most surficial exposures too weathered to retain compaction; varied levels of sorting; clasts rounded to subangular; northern sourced. Association with pre-Vashon Olympia and Yelm ice lobes varies. Most exposures of unit Qpd are weathered into surficial soil in which sedimentary structures have been obliterated by soil development. Where the unit is thin, diagnostic properties in some exposures include less weathering and more angular (till) clods than in underlying deposits, such as a red, fat clay substrate (of unknown origin) at significant site S2. Beneath Mima, Baker, and Grand Mound Prairies, unit Qpd is widely inferred from well records, such as at W6 (map and Cross Section A–A′), where the top of unit Qpd likely includes 11 ft of lodgment till.

Alpine drift

Qapo$_{lh}$ — **Logan Hill Formation (Pleistocene)**—Secondary clay soil, grading to parent material of pebble gravel and sand with matrix of sandy, silty clay at depths >10–30 ft; interbeds of silt and clay (Snavely and others, 1951, 1958) not observed in map area; multicolored, red to reddish brown and pale brown to yellowish brown; strongly weathered to rotten; mildly to moderately compact, poorly indurated; clasts mostly well rounded and equant to oblate, with imbrication weakly suggested in some exposures. Large numbers of intermediate to felsic igneous rocks and much fewer mafic igneous rocks in clast count C35 broadly resemble clast counts of Logan Hill Formation south of the map area (C7, C8, C12, C13, and C16 of Sadowski and others, 2019); a high content of metamorphic rocks, quartz, and chert may indicate that less resistant lithologies have weathered out at clast count site C38. Unit Qapo$_{lh}$ is approximately 50–80 ft thick based on well records and slope exposures. The unit forms a largely flat surface on Michigan Hill and unconformably overlies bedrock. U-Pb analysis of detrital zircons at GD6 yielded an age of <1.9 ±0.8 Ma, consistent with U-Pb ages from Logan Hill Formation farther south (Sadowski and others, 2018, 2019), but GD6 stands alone in lacking Miocene zircons, suggesting that the unit at Logan Hill accessed a different sedimentary source. The Logan Hill Formation is interpreted as Cascade Mountains-sourced outwash (Snavely and others, 1958).

Quaternary To Eocene Continental Deposits

QEcf, QEcf$_s$ — **Terrestrial weathering clay**—Clay, silty clay, sandy clay, and saprolite, interpreted as weathering product of mostly Crescent Formation basalt, or McIntosh Formation siltstone and sandstone where mapped as unit QEcf$_s$; locally includes corestones of basalt (in unit QEcf) or sedimentary rock (in unit QEcf$_s$); east of the glacial ice limit, and in some valleys farther west, unit likely includes weathering products of pre-Vashon drift; colored red, brown, pink, white, yellow to orange; loose near surface; homogeneous except where saprolite preserves primary structure; >44% halloysite and 15–26% goethite where basalt-based, >60% smectite (nontronite) in sedimentary rock-based facies; drift enriches the unit with quartz, plagioclase, and K-feldspar (orthoclase) at the expense of nontronite, goethite, and halloysite (Polenz and others, 2017). Unit QEcf is mapped in the Black Hills near the northwest corner of the map area, where it fully conceals bedrock; exposures north of the map area suggest the unit is commonly >30 ft thick (Polenz and others, 2017). Unit age is constrained to less than its parent material.

Tertiary Volcanic and Sedimentary Bedrock

Mc$_w$ — **Wilkes Formation (Miocene)**—Semi-consolidated pebble gravel and sand; light gray to medium brown; weakly to moderately cemented sand; matrix is very coarse to fine-grained sand with subangular to subrounded pebbles and cobbles; moderately to well sorted; moderately to strongly weathered, but less weathered than Logan Hill Formation; tentatively mapped based on similarity of lithologies and weathering to clast counts from Wilkes Formation farther south (Sadowski and others, 2018, 2019); observed in a single exposure at C30, where it was exposed mid-cliff, resting on Lincoln Creek Formation siltstone; inferred nearby from midslope benches and stream channel landforms that suggest the unit erodes differently from sediments above and bedrock below. Carbonized plant matter has elsewhere been described as abundant in the Wilkes Formation (Roberts, 1958; Snavely and others, 1958) but was not observed here—perhaps only due to poor access to the mid-cliff exposure. Maximum limiting ages from the unit south of the map area range from <13.6 ±1.9 to <6.2 ±1.0 Ma.

Mm$_a$ — **Astoria(?) Formation (Miocene)**—Marine siltstone, shale, sandstone, isolated interbeds of volcaniclastic conglomerate, and detrital, carbonised wood; bluish-greenish gray, weathers yellowish tan to pale brown, light orange-brown and dark grayish brown; crumbly; unbedded; siltstone facies contains about 5% coarse sand; otherwise well sorted; quartz rich with volcanic lithic fragments. Three–5% dark minerals in most exposures confirm Snavely and others' (1958) assertion that heavy minerals in the Astoria Formation are "much more abundant" than in older sedimentary rocks of the map area, but some upper Lincoln Creek Formation outcrops, such as at GD9 and G45, revealed a similar black mineral content. Volcaniclastic conglomerate interbeds are inferred from isolated clusters of pebbles emerging from otherwise homogeneous, clayey, siltstone-derived soil at G30 and G36–G38. Geochemical similarity of the pebbles to volcanic rocks of Grays River (Phillips and others, 1989; Chan and others, 2012) suggests that the conglomerate interbeds are derived from that unit in the Willapa Hills south and southwest of the map area. Astoria(?) Formation text references are queried because correlation to the now non-existent type section in Oregon (Howe, 1926; Beaulieu, 1971) is not testable.

Observed exposures suggest that Astoria(?) Formation in the map area more likely corresponds to Snavely and others' (1958) lower unit of fossiliferous sandstone with siltstone lenses than their upper unit of fine-grained arkosic sandstone with mottled quartz pebbles. The mapped extent of Astoria(?) Formation and a well log at W32 suggest more than 130 ft unit thickness. The unit is mapped along the Centralia syncline from the western flank of Michigan Hill to the southern map edge. Some of the unit extent is inferred from midslope benches and stream channel landforms that suggest the unit erodes differently from deposits above and below. Similarity of some exposures and similar maximum depositional ages of detrital zircons at GD10 (Astoria(?) Formation) and GD9 (Lincoln Creek Formation) suggest that Astoria(?) Formation may locally be a lateral equivalent of the upper part of the Lincoln Creek Formation, but different zircon spectra suggest they are derived at least partly from different sources.

No contact with Lincoln Creek Formation was observed, and Astoria(?) Formation is therefore queried where laterally adjacent to Lincoln Creek Formation. Astoria(?) Formation in the map area appears laterally continuous with middle Miocene Astoria(?) Formation at age site GD6 of Sadowski and others (2019) 1,900 ft south of the map area. Localized thinning or absence of the underlying Lincoln Creek Formation along the southern map edge suggests that much (or all?) of the Astoria(?) Formation in the map area rests on an unconformity. If so, then lateral equivalence(?) to upper Lincoln Creek Formation on western Michigan Hill seems unlikely.

This unit was was mapped as Astoria(?) Formation because (1) Snavely and others (1958) mapped it in the area; (2) the detrital zircon U-Pb age spectrum at age site GD10 resembles that of Astoria(?) Formation a few miles south of the map area (age site GD4 of Sadowski and others, 2019) and does not resemble spectra from the Lincoln Creek Formation type section (GD9, GD11); and (3) carbonified detrital wood was observed at GD9 and suggested upsection thereof by "Coal Sandstone" in well log (W32), and is common in the (marine) Astoria(?) Formation but not in the Lincoln Creek Formation.

ΦEm$_{lc}$ — **Lincoln Creek Formation (Miocene to Eocene)**—Siltstone and sandstone, locally tuffaceous and fossiliferous; greenish gray to pale gray to ivory; moderately weathered with tan to orange weathered faces observed locally; siltstone mostly unbedded; sandstone unbedded to bedded; locally hackly and spheroidally weathered; calcareous interbeds commonly form concretions. Unit thickness in the map area has been estimated at 1,200 ft at the type section between Galvin and Helsing Junction (Beikman and others, 1967), plus 800 ft in the subsurface at HC4 (Snavely and others, 1958), suggesting at least 2,000 ft total thickness, but the bedding orientations and geophysical modeling that underpin Cross Section A–A′ suggest only 1,600 ft.

Unit ΦEm$_{lc}$ is relatively widely exposed on Michigan Hill. It is equivalent in the map area to the tuffaceous siltstone facies of Snavely and others' (1958) Lincoln Formation, except for a 4 ft thick interbed of basaltic sandstone (clast count site C36) and 15 ft of volcaniclastic conglomerate at C39, both near the southern map edge. These are equivalent to Snavely and others' (1958, p. 38) basaltic sandstone (to conglomerate) facies. Unit ΦEm$_{lc}$ has yielded many biostratigraphy records in the map area (GD30–42, 46–65, 69–95, 97–102) and cetacean fossils in at least two locations (Peredo and Pyenson, 2017; Larry Weaver, Dream Weavers Real Estate, written commun., 2019). Detrital zircons from tuffaceous rock at age site GD11 in the type section near Galvin suggest a <28.6 ±2.1 Ma maximum depositional age that is close to a depositional age. Bedding dips suggest that the type section exposures farther north near HC4 are older. A 36.7 ±0.3 Ma zircon population from tuff in the Lincoln Creek Formation (Sadowski and others, 2018) and a 36.6 ±0.4 Ma ^{40}Ar/^{39}Ar age from (ostensibly older) volcanic rocks of Grays River (Wells and others, 2014; Nesbitt, 2018) constrain the age of the base of the formation. Fossils and U-Pb age GD9 (<20.3±1.7 Ma) document inclusion of Miocene rocks in the type section. Unit ΦEm$_{lc}$ unconformably overlies Skookumchuck Formation and is (mostly?) older than Astoria(?) Formation.

En$_{sk}$ — **Skookumchuck Formation (late to middle Eocene)**—Siltstone and sandstone, micaceous (>5%), locally coal-bearing; gray or bluish gray, weathers olive-tan to pale yellowish brown, forms reddish orange silty and clayey soil; fine to medium grained; angular to rounded; moderately to well sorted; poorly to well bedded with bedding locally best signaled by preferential mica orientations; locally contains plant material, macrofossils and (or) isolated but common, rounded concretions; usually contains more mica and fewer opaque minerals than the McIntosh Formation. Unit thickness of 2,200 ft is inferred along the eastern map boundary based on prior mapping (Polenz and others, 2018). Combined modeling of gravity and magnetic data suggests unit thickening to 2,500 ft within the map area. Unit En$_{sk}$ is exposed southwest of the Scammon Creek fault near the southwest corner of the map, and in the eastern half of the map area between the Kopiah and Rochester faults, where the Dalton No. 2 oil well (HC3) was interpreted as Skookumchuck Formation to 1,700 ft below the surface (Rau, WGS, unpub. records, 1963). Marginal-marine to brackish-water fossils at GD28 and delicate plant fragment fossils at GD24 conform to Snavely and others' (1951) unit definition as marine to brackish (deltaic) and nonmarine. Although contact relations were not observed in the map area, Pease and Hoover (1957) indicated that the McIntosh and lower Skookumchuck Formations interfinger west of the map area. Detrital zircon U-Pb ages constrain lower Skookumchuck Formation to <41.4 ±1.4 Ma at age site GD12 (Table M2; Polenz and others, 2018).

Em$_{2m}$ — **McIntosh Formation (middle Eocene)**—Volcanic lithic marine siltstone and sandstone, commonly tuffaceous; fine to medium grained; gray-green, weathers yellowish brown, buff, and medium brown; most grains are feldspar; commonly contains green to colorless grains in brownish yellow, fine-grained matrix rich with opaque and altered minerals, usually with more opaque minerals and less mica than Skookumchuck Formation. Exposures of the unit appear to onlap Crescent Formation north of the Black River, although the contact was not observed. Unit distribution there suggests a unit thickness >100 ft; exposures elsewhere in the map area are small, but 1,255 ft of "upper" to "middle" McIntosh Formation was interpreted at the base of the Dalton No. 2 oil well (HC3)(Rau, WGS, unpub. records, 1963), and we infer about 4,000 ft of similar rocks along Cross Section A–A′, based on combined modeling of gravity and magnetics and a regional maximum unit thickness of 4,500 ft (Snavely and others, 1958). Because unit Em$_{2m}$ is of middle to upper Eocene age (Snavely and others, 1959), some of the 4,000 ft section inferred along Cross Section A–A′ may range to lower Eocene rocks similar to those mapped east of the map area as part of a downsection-expanded McIntosh Formation unit Em$_m$ in the Bannse No. 1 well (Polenz and others, 2018). Aside from unspecified fragments of leaf and wood at GD15, no McIntosh Formation macrofossils were found in the Rochester quadrangle; Tertiary shallow-water benthic foraminifera found in the quadrangle and nearby are not age-diagnostic (Table DS2; Snavely and others, 1958; Logan and others, 2009).

Ev$_c$ — **Crescent Formation**—Plagioclase-pyroxene tholeiitic basalt; commonly with amygdules of zeolite, chlorite, calcite, or quartz; dark gray with greenish tint, weathers brown or reddish and variegated along altered contact zones; exposures include breccias, columnar-jointed flows or sills, and possibly dikes. Zeolite and chlorite or chloritoid matrix alteration is pervasive. Angular sandstone and siltstone float in the northeastern valley wall at significant site S3 suggests interbedded Crescent Formation sedimentary rock. Radiometric ages constrain the Crescent Formation in the southern Black Hills to between ~55 and 47.4 ±0.2 Ma (Polenz and others, 2017; Eddy and others, 2017, Wells and others, 2014). Ulatisian- or lower Narizian-age fossils from the southern Black Hills are consistent with this age range (Polenz and others, 2017). Two paleomagnetic measurement locations document magnetically reversed Crescent Formation basalt in the map area (M1, M2).

ACKNOWLEDGMENTS

We thank: Ruth Martin for microfossil analysis and assistance with fossil sample collection; Kevin Hansen (Thurston County) for samples and notes from groundwater monitoring wells; Tim Walsh, Pat Pringle, Josh Logan, and Hank Schasse (all WGS retired) for fielding questions about prior mapping and other issues; all WGS active staff for their edits and guidance; Pat Pringle (WGS retired), Joe Rocchio, Brandon Austin, Matt Provencher, and Tynan Ramm-Granberg (all DNR), John Fleckenstein (DNR retired), and Paul Bakke (USFWS retired) for diverse assistance with plant samples; Cody Duckworth for assistance with field work; Larry Weaver and Diana Holbrook for land access and samples and suggestions; Jerri Parrish, Steve Weber, Larry and Linda Remmers, Dave Seiler, Elvin Borg, John and Krista Geist, The Nature Conservancy, Port Blakely Tree Farms, Bascom Pacific, LLC., Hemphill O'Neill Co., and countless other kind landowners and residents for land access.

REFERENCES

Anderson, M. L.; Lau, T. R.; von Dassow, W. A.; Reedy, T. J.; Staisch, L. M.; Cakir, Recep; Sadowski, A. J.; Polenz, Michael; Becerra, R. I.; Toth, C. H.; Steely, A. N.; Walsh, T. J.; Norman, D. K.; Sherrod, B. L., 2018, The Doty fault network: 3D regional deformation applied to seismic hazard characterization in the forearc of Washington State [abstract]: American Geophysical Union (AGU) Fall Meeting, Washington, D.C., Dec. 10–14, 2018. [https://www.dnr.wa.gov/publications/ger_presentations_agu_2018_anderson.pdf?wexifq]

Anderson, Tom, 2002, Correction of common lead in U-Pb analyses that do not report 204Pb: Chemical Geology, v. 192, issue 1-2, p. 59–79. [https://doi.org/10.1016/S0009-2541(02)00195-X]

Beaulieu, J. D., 1971, Geologic formations of western Oregon (west of longitude 121° 30′): Oregon Department of Geology and Mineral Industries Bulletin 70, 72 p. [http://www.oregongeology.org/pubs/B/B-070.pdf]

Beikman, H. M.; Rau, W. W.; Wagner, H. C., 1967, The Lincoln Creek Formation, Grays Harbor basin, southwestern Washington: U.S. Geological Survey Bulletin 1244-I, 14 p. [http://pubs.er.usgs.gov/publication/b1244I]

Blakely, R. J.; Wells, R. E.; Sherrod, B. L.; Brocher, T. M., 2016, Segmentation of the Cascadia forearc in southwestern Washington—evidence from new potential-field data [abstract]: AGU Fall Meeting, 12–16 December, 2016, abstract #GP34A-04.

Boynton, W.V., 1984, Cosmochemistry of the rare earth elements: Meteorite studies. *In* Henderson, P., editors, Rare Earth Element Geochemistry: vol. 2, Amsterdam, Netherlands, Elsevier, p. 63–114.

Bretz, J. H., 1913, Glaciation of the Puget Sound region: Washington Geological Survey Bulletin 8, 244 p., 3 plates. [http://www.dnr.wa.gov/publications/ger_b8_glaciation_pugetsound.pdf]

Bromery, R. W., 1962, Aeromagnetic and gravimetric interpretation of the geology of the Malone, Rochester, Pe Ell, and Adna quadrangles, Pacific, Lewis, Grays Harbor, and Thurston Counties, Washington: American University Master of Science thesis, 44 p., 4 plates.

Burnham, J. L. H.; Johnson, D. L., editors, 2012, Mima Mounds—The case for polygenesis and bioturbation: Geological Society of America Special Paper 490, 205 p.

Chan, C. F.; Tepper, J. H.; Nelson, B. K., 2012, Petrology of the Grays River volcanics, southwest Washington: Plume-influenced slab window magmatism in the Cascadia forearc: Geological Society of America Bulletin, v. 124, p. 1324–1338.

Contreras, T. A.; Spangler, Eleanor; Fusso, L. A.; Reioux, D. A.; Legorreta Paulín, Gabriel; Pringle, P. T.; Carson, R. J.; Lindstrum, E. F.; Clark, K. P.; Tepper, J. H.; Pileggi, Domenico; Mahan, S. A., 2012, Geologic map of the Eldon 7.5-minute quadrangle, Jefferson, Kitsap, and Mason Counties, Washington: Washington Division of Geology and Earth Resources Map Series 2012-03, 1 sheet, scale 1:24,000, with 60 p. text.

Eddy, M. P.; Clark, K. P; Polenz, Michael, 2017, Age and volcanic stratigraphy of the Eocene Siletzia oceanic plateau in Washington and Vancouver Island: Lithosphere, v. 9, no. 4., p. 652–664. [https://doi.org/10.1130/L650.1.]

Gabet, E. J.; Burnham, J. L. H.; Perron. J. T., 2016, Critiques of the seismic hypothesis and the vegetation stabilization hypothesis for the formation of Mima mounds along the western coast of the U.S.: Geomorphology, v. 269, p. 40–42. [https://doi.org/10.1016/j.geomorph.2016.06.032]

Howe, H. V., 1926, Astoria—Mid-Tertic type of Pacific coast: Pan-American Geologist, v. 45, no. 4, p. 295–306.

Irvine, T. N.; Baragar, W. R. A., 1971, A guide to the chemical classification of the common volcanic rocks: Canadian Journal of Earth Sciences, v. 8, p. 523–548. [https://doi.org/10.1139/e71-055]

Jackson, S. E.; Pearson, N. J.; Griffin, W. L.; Belousava, E. A., 2004, The application of laser ablation-inductively coupled plasma-mass spectrometery to in situ U-Pb zircon geochronology, Chemical Geology, v. 211, p. 47–69. [https://doi.org/10.1016/j.chemgeo.2004.06.017]

Johnson, S. Y.; Blakely, R. J.; Stephenson, W. J.; Dadisman, S. V.; Fisher, M. A., 2004, Active shortening of the Cascadia forearc and implications for seismic hazards of the Puget Lowland: Tectonics, v. 23, no. TC1011, 27 p. [https://doi.org/10.1029/2003TC001507]

Lau, T. R.; Anderson, M. L.; Polenz, Michael; Sadowski, A. J.; Becerra, R. I.; Toth, C. H.; Cakir, Recep; von Dassow, W. A.; Reedy, T. J.; Staisch, L. M.; Steely, A. N., Walsh, T. J.; Sherrod, B. L., 2018, Integrated geophysical investigation and 3D fault characterization of the Rochester and Adna 7.5-minute quadrangles, Thurston and Lewis Counties, Washington [poster]: American Geophysical Union (AGU) Fall Meeting, Washington, D.C, Dec. 10-14, 2018.[https://www.dnr.wa.gov/publications/ger_presentations_agu_2018_lau.pdf?wexifq]

Le Bas, M. J.; Le Maitre, R. W.; Streckeisen, A. L.; Zanettin, Bruno, 1986, A chemical classification of volcanic rocks based on the total alkali-silica diagram: Journal of Petrology, v. 27, part 3, p. 745-750. [https://doi.org/10.1093/petrology/27.3.745]

Logan, R. L., compiler, 1987, Geologic map of the Chehalis River and Westport quadrangles, Washington: Washington Division of Geology and Earth Resources Open File Report 87-8, 16 p., 1 plate, scale 1:100,000. [http://www.dnr.wa.gov/Publications/ger_ofr87-8_geol_map_chehalisriver_westport_100k.zip]

Logan, R. L.; Walsh, T. J., 2009, Mima mounds formation and their implications for climate change [abstract]. *In* Northwest Scientific Association, The Pacific Northwest in a changing environment—Northwest Scientific Association 81st annual meeting; Program with abstracts: Northwest Scientific Association, p. 38–39. [http://www.northwestscience.org/Resources/Final%20Annual%20Meeting%20Abstracts%20and%20Programs/2009%20NWSA%20Program%20and%20Abstracts.pdf]

Logan, R. L.; Walsh, T. J.; Stanton, B. W.; Sarikhan, I. Y., 2009, Geologic map of the Maytown 7.5-minute quadrangle, Thurston County, Washington: Washington Division of Geology and Earth Resources Geologic Map GM-72, 1 sheet, scale 1:24,000. [http://www.dnr.wa.gov/Publications/ger_gm72_geol_map_maytown_24k.pdf]

Ludwig, K. R., 2003, User's manual for Isoplot 3.00. A geochronological toolkit for Microsoft Excel: Berkely Geochronology Center, Special Publication no. 4a, Berkeley, California.

McCaffrey, Robert; King, R. W.; Payne, S. J.; Lancaster, Matthew, 2013, Active tectonics of northwestern U.S. inferred from GPS-derived surface velocities: Journal of Geophysical Research Solid Earth, v. 118, issue no. 2, p. 709–723. [http://onlinelibrary.wiley.com/doi/10.1029/2012JB009473/epdf]

Nesbitt, E. A., 2018, Cenozoic marine formations of Washington and Oregon—An annotated catalogue: PaleoBios, v. 35, 20 p., [https://escholarship.org/uc/item/04q5f9cr]

Noble, J. B.; Wallace, E. F., 1966, Geology and ground-water resources of Thurston County, Washington; Volume 2: Washington Division of Water Resources Water-Supply Bulletin 10, 141 p., 5 plates. [http://www.ecy.wa.gov/programs/eap/wsb/wsb_All.html]

Pease, M. H., Jr.; Hoover, Linn, Jr., 1957, Geology of the Doty–Minot Peak area, Washington: U.S. Geological Survey Oil and Gas Investigations Map OM-188, 1 sheet, scale 1:62,500. [http://pubs.er.usgs.gov/publication/om188]

Pena, L. D.; Goldstein, S. L., 2014, Thermohaline circulation crisis and impacts during the mid-Pleistocene transition: Science, v. 345, no. 6194, p. 318–322. [https://doi.org/10.1126/science.1249770]

Peredo, C. M.; Pyenson, N. D, 2017, *Salishicetus meadi*, a new aetiocetid from the late Oligocene of Washington State and implications for feeding transitions in early mysticete evolution: Royal Society Open Science, v. 5, no. 4. [https://doi.org/10.1098/rsos.172336; supplementary data at https://doi.org/10.6084/m9.figshare.c.4056575]

Petrus, J. A.; Kamber, B. S., 2012, VizualAge: A novel approach to laser ablation ICP-MS U-Pb geochronology data reduction: Geostandards and Geoanalytical Research, v. 36, no. 3, p. 247–270. [https://doi.org/10.1111/j.1751-908X.2012.00158.x]

Phillips, W. M.; Walsh, T. J.; Hagen, R. A., 1989, Eocene transition from oceanic to arc volcanism, southwest Washington. *In* Muffler, L. J. P.; Weaver, C. S.; Blackwell, D. D., editors, Proceedings of workshop XLIV—Geological, geophysical, and tectonic setting of the Cascade Range: U.S. Geological Survey Open-File Report 89-178, p. 199–256. [http://pubs.er.usgs.gov/publication/ofr89178]

Polenz, Michael; Favia, J. G.; Hubert, I. J.; Legorreta Paulín, Gabriel; Cakir, Recep, 2015, Geologic map of the Port Ludlow and southern half of the Hansville 7.5-minute quadrangles, Kitsap and Jefferson Counties, Washington: Washington Division of Geology and Earth Resources Map Series 2015-02, 1 sheet, scale 1:24,000, 40 p. text. [http://www.dnr.wa.gov/publications/ger_ms2015-02_geol_map_port_ludlow_hansville_24k.zip]

Polenz, Michael; Gordon, H. O.; Hubert, I. J.; Contreras, T. A.; Patton, A. I.; Legorreta Paulín, Gabriel; Cakir, Recep, 2014, Geologic map of the Center 7.5-minute quadrangle, Jefferson County, Washington: Washington Division of Geology and Earth Resources Map Series 2014-02, 1 sheet, scale 1:24,000, with 35 p. text. [http://www.dnr.wa.gov/Publications/ger_ms2014-02_geol_map_center_24k.zip]

Polenz, Michael; Miller, B. A.; Davies, Nigel; Perry, B. B.; Hughes, J. F.; Clark, K. P.; Walsh, T. J.; Tepper, J. H.; Carson, R. J., 2012a, Analytical data from the Hoodsport 7.5-minute quadrangle, Mason County, Washington—Supplement to Open File Report 2011-3: Washington Division of Geology and Earth Resources Open File Report 2011-4, 42 p. [http://www.dnr.wa.gov/Publications/ger_ofr2011-4_hoodsport_supplement.pdf]

Polenz, Michael; Ostrom, B. A.; Lau, T. R.; Sadowski, A. J.; Blanks-Bennett, A. L.; Cakir, Recep; Tepper, J. H.; Legorreta Paulín, Gabriel; Nesbitt, Elizabeth; DuFrane, S. A., 2018, Geologic map of the Violet Prairie 7.5-minute quadrangle, Thurston and Lewis Counties, Washington: Washington Geological Survey Map Series 2018-04, 1 sheet, scale 1:24,000, 41 p. text. [http://www.dnr.wa.gov/publications/ger_ms2018-04_geol_map_violet_prairie_24k.zip]

Polenz, Michael; Spangler, Eleanor; Fusso, Logan A.; Reioux, David A.; Cole, Ryan A.; Walsh, Timothy J.; Cakir, Recep; Clark, Kenneth P.; Tepper, Jeffrey H.; Carson, Robert J.; Pileggi, Domenico; Mahan, Shannon A., 2012b, Geologic map of the Brinnon 7.5-minute quadrangle, Jefferson and Kitsap Counties, Washington: Washington Division of Geology and Earth Resources Map Series 2012-02, 1 sheet, scale 1:24,000, with 47 p. text. [https://fortress.wa.gov/dnr/geologydata/pdf3d/ger_ms2012-02_geol_map_brinnon_24k_3D.pdf]

Polenz, Michael; Vermeer, J. L.; Legorreta Paulín, Gabriel; Tepper, J. H.; Mahan, S. A.; Cakir, Recep, 2017, Geologic map of the Littlerock 7.5-minute quadrangle, Thurston County, Washington: Washington Geological Survey Map Series 2017-01, 1 sheet, scale 1:24,000, 36 p. text. [http://www.dnr.wa.gov/publications/ger_ms2017-01_geol_map_littlerock_24k.zip]

Roberts, A. E., 1958, Geology and coal resources of the Toledo–Castle Rock district, Cowlitz and Lewis Counties, Washington: U.S. Geological Survey Bulletin 1062, 71 p., 6 plates. [https://pubs.er.usgs.gov/publication/b1062]

Sadowski, A. J.; Becerra, R. I.; Toth, C. H.; Polenz, Michael; Anderson, M. L.; Lau, T. R.; Nesbitt, E. A.; Tepper, J. H.; DuFrane, S. A., 2019, Geologic map of the Adna 7.5-minute quadrangle, Lewis County, Washington: Washington Geological Survey Map Series 2019-01, 1 sheet, scale 1:24,000. [http://www.dnr.wa.gov/publications/ger_ms2019-01_geol_map_adna_24k.zip]

Sadowski, A. J.; Keller, W. E.; Polenz, Michael; Lau, T. R.; Cakir, Recep; Nesbitt, Elizabeth; Tepper, J. H.; DuFrane, S. A.; Legorreta Paulín, Gabriel, 2018, Geologic map of the Centralia 7.5-minute quadrangle, Lewis County, Washington: Washington Geological Survey Map Series 2018-05, 1 sheet, scale 1:24,000, 43 p. text. [http://www.dnr.wa.gov/publications/ger_ms2018-05_geol_map_centralia_24k.zip]

Sherrod, B. L.; Blakely, R. J.; Weaver, C. S.; Kelsey, H. M.; Barnett, Elizabeth; Liberty, Lee; Meagher, K. L.; Pape, Kristin, 2008, Finding concealed active faults—Extending the southern Whidbey Island fault across the Puget Lowland, Washington: Journal of Geophysical Research, v. 113, no. B05313. [https://doi.org/10.1029/2007JB005060]

Sláma, Jiří; Košler, Jan; Condon, D. J.; Crowley, J. L.; Gerdes, Axel; Hanchar, J. M.; Horstwood, M. S. A.; Morris, G. A.; Nasdala, Lutz; Norberg, Nicholas; Schaltegger, Urs; Schoene, Blair; Tubrett, M. N.; Whitehouse, M. J., 2018, Plešovice zircon—A new natural reference material for U-Pb and Hf isotopic microanalysis: Chemical Geology, v. 249, no. 1-2, p. 1–35. [https://doi.org/10.1016/j.chemgeo.2007.11.005]

Snavely, P. D., Jr.; Brown, R. D., Jr.; Roberts, A. E.; Rau, W. W., Schopf, J. M., 1958, Geology and coal resources of the Centralia–Chehalis district, Washington, with a section on microscopical character of Centralia–Chehalis coal: U.S. Geological Survey Bulletin 1053, 159 p., 6 plates. [http://pubs.er.usgs.gov/usgspubs/b/b1053]

Snavely, P. D., Jr.; Rau, W. W.; Hoover, Linn, Jr.; Roberts, A. E., 1959, McIntosh Formation, Centralia–Chehalis coal district, Washington. In Washington Division of Mines and Geology, Tertiary stratigraphic papers, southwestern Washington: Washington Division of Mines and Geology Reprint 3, 10 p. [http://www.dnr.wa.gov/publications/ger_reprint3_strat_papers_sw_wa.pdf]

Snavely, P. D., Jr.; Roberts, A. E.; Hoover, Linn, Jr.; Pease, M. H., Jr., 1951, Geology of the eastern part of the Centralia–Chehalis coal district, Lewis and Thurston Counties, Washington: U.S. Geological Survey Coal Investigations Map C8, 2 sheets, scale 1:31,680. [http://pubs.er.usgs.gov/publication/coal8]

Sun, S.-s; McDonough, W. F., 1989, Chemical and isotopic systematics of oceanic basalts—Implications for mantle composition and processes. *In* Saunders, A.D.; Norry, M.J., editors, Magmatism in the Ocean Basins: Geological Society of London Special Publication 42, p. 313–345.

Walsh, T. J.; Logan, R. L., 2005, Geologic map of the East Olympia 7.5-minute quadrangle, Thurston County, Washington: Washington Division of Geology and Earth Resources Geologic Map GM-56, 1 sheet, scale 1:24,000. [http://www.dnr.wa.gov/Publications/ger_gm56_geol_map_eastolympia_24k.pdf]

Walsh, T. J.; Korosec, M. A.; Phillips, W. M.; Logan, R. L.; Schasse, H. W., 1987, Geologic map of Washington—Southwest quadrant: Washington Division of Geology and Earth Resources Geologic Map GM-34, 2 sheets, scale 1:250,000, with 28 p. text. [http://www.dnr.wa.gov/Publications/ger_gm34_geol_map_sw_wa_250k.pdf]

Washburn, A. L., 1988, Mima mounds—An evaluation of proposed origins with special reference to the Puget Lowland: Washington Division of Geology and Earth Resources Report of Investigations 29, 53 p. [http://www.dnr.wa.gov/publications/ger_ri29_mima_mounds.pdf]

Washington Public Power Supply System, 1974, WPPSS Nuclear Project no. 3—Preliminary safety analysis report, Volume 3B: Washington Public Power Supply System, 1 v.

Wallace, E. F.; Molenaar, Dee, 1961, Geology and ground-water resources of Thurston County, Washington, Volume 1: Washington Division of Water Resources Water Supply Bulletin 10, v. 1, 254 p., 2 plates. [http://www.ecy.wa.gov/programs/eap/wsb/wsb_All.html]

Weigle, J. M.; Foxworthy, B. L., 1962, Geology and ground-water resources of west-central Lewis County, Washington: Washington Division of Water Resources Water Supply Bulletin 17, 248 p., 5 plates. [http://www.ecy.wa.gov/programs/eap/wsb/wsb_All.html]

Wells, Ray; Bukry, David; Friedman, Richard; Pyle, Doug; Duncan, Robert; Haeussler, Peter; Wooden, Joe, 2014, Geologic history of Siletzia, a large igneous province in the Oregon and Washington Coast Range—Correlation to the geomagnetic polarity time scale and implications for a long-lived Yellowstone hotspot: Geosphere, v. 10, no. 4, p. 692–719. [https://doi.org/10.1130/GES01018.1]

Wells, R. E., McCaffrey, R., 2013, Steady rotation of the Cascade arc: Geology, v. 41, no. 9, p. 1027–1030. [https://doi.org/10.1130/G34514.1]

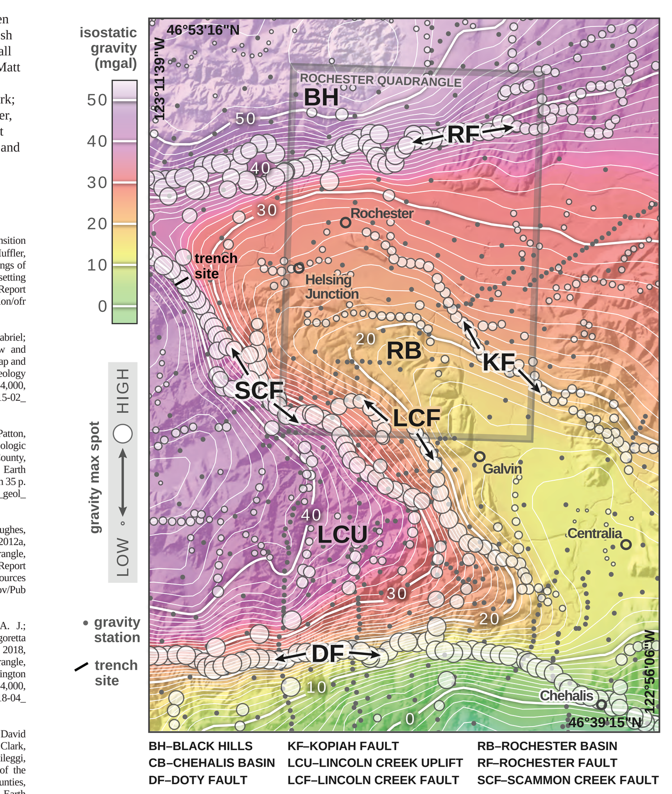

Figure M1. Geophysical mapping for the Rochester quadrangle. Isostatic gravity grid with 1 mGal contours on a lidar bare-earth hillshade. Gravity stations are shown as gray dots. Gravity max spots are shown as partially transparent white circles, where relative size of the circle is proportional to the magnitude of the gravity gradient. Trench site (solid black line) marks Scammon Creek fault investigation locality (Washington Public Power Supply System, 1974).

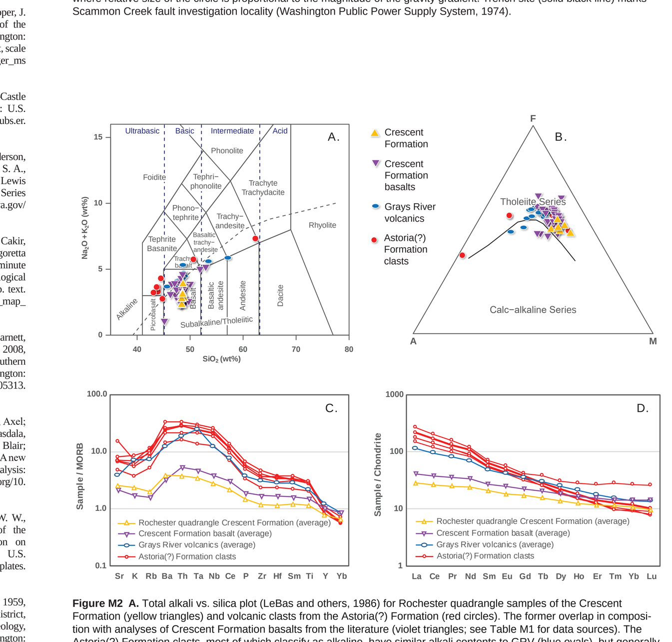

Figure M2 A. Total alkali vs. silica plot (LeBas and others, 1986) for Rochester quadrangle samples of the Crescent Formation (yellow triangles) and volcanic clasts from the Astoria(?) Formation (red circles). The former overlap in composition with analyses of Crescent Formation basalts from the literature (violet triangles; see Table M1 for data sources). The Astoria(?) Formation clasts, most of which classify as alkaline, have similar alkali contents to GRV (blue ovals), but generally lower silica. **B.** AFM diagram (Irvine and Baragar, 1971) showing that all volcanic rock samples from the Rochester quadrangle classify as tholeiitic. Symbols are the same as in Figure M1A. **C.** MORB-normalized spidergrams (Sun and McDonough, 1989) illustrating the similarities between Rochester quadrangle basalts and Crescent Formation rocks and between Astoria(?) Formation clasts and GRV. Note also that none of the Rochester quadrangle samples display depletions in Ta and Nb that are characteristic of Cascade arc rocks. Data sources listed in Table M1. **D.** Rare earth element (REE) data (normalized to the recommended chondrite values of Boynton, 1984). Note the similar, unfractionated patterns of the Rochester quadrangle and other Crescent Formation samples and the steeper profiles shared by the Astoria(?) Formation clasts and GRV. Data sources listed in Table M1.

Table M1. Chemical comparisons of Rochester quadrangle (RQ) samples with Crescent Formation basalts and volcanic rocks of Grays River (GRV). Average Crescent Formation data (with 1σ standard deviation in parentheses) based on 42 analyses from the Olympic Mountains and Black Hills (Contreras and others, 2012; Polenz and others, 2012a, 2012b, 2014, 2017). Average GRV data compiled from Chan and others (2012).

	Rochester Quadrangle Crescent Formation (average)	Crescent Formation (average)	Rochester Quadrangle Astoria(?) Formation clasts (average)	Grays River volcanics (average)
SiO_2 (wt. %)	48.6 ±0.2	48.3 ±1.0	45.6 ±3.0	48.9 ±3.3
TiO_2 (wt. %)	1.7 ±0.3	2.3 ±0.5	3.9 ±0.6	3.2 ±0.5
K_2O (wt. %)	0.6 ±0.03	0.3 ±0.1	1.1 ±0.4	1.1 ±0.5
Mg-number	0.6 ±0.03	0.5 ±0.1	0.5 ±0.1	0.4 ±0.2
La/YbN	3.0 ±0.4	3.0 ±0.6	17.1 ±4.2	8.4 ±0.6
Nb (ppm)	9.7 ±3	13.4 ±5	74.5 ±14.9	43.0 ±11.5

Table M2. Summary of chronometric ages from the Rochester quadrangle. The reported age for each U-Pb sample is from the single, youngest zircon, except for GD12[1]. See Data Supplement for detailed analytical results and biostratigraphic ages.

Sample	Unit symbol	Location	Method	Result
Age control samples				
GD1	Qls? (or ml)	sec. 16, T15N R3W	^{14}C	150 ±30 ^{14}C years BP
GD2	Qgog	sec. 32, T16N R3W	^{14}C	280 ±30 ^{14}C years BP
GD3	Qoa	sec. 11, T15N R3W	U-Pb	0.3 ±0.5 Ma
GD4	Qpo	sec. 24, T16N R3W	U-Pb	1.4 ±0.2 Ma
GD5	Qpo	sec. 24, T16N R3W	U-Pb	0.8 ±1.0 Ma
GD6	Qapo$_{lh}$	sec. 20, T15N R3W	U-Pb	1.9 ±0.8 Ma
GD7	Qpd	sec. 22, T16N R3W	U-Pb	3.0 ±0.7 Ma
GD8	Qpd	sec. 25, T16N R3W	U-Pb	2.4 ±1.6 Ma
GD9	ΦEm$_{lc}$	sec. 7, T15N R3W	U-Pb	20.3 ±1.7 Ma
GD10	Mm$_a$	sec. 24, T15N R4W	U-Pb	22.1 ±1.5 Ma
GD11	ΦEm$_{lc}$	sec. 26, T15N R3W	U-Pb	28.6 ±2.1 Ma
GD12	En$_{sk}$	sec. 12, T15N R3W	U-Pb	No older than 41.4 ±1.4 Ma[1]
GD13	ΦEm$_{lc}$	sec. 22, T15N R3W	U-Pb	Age analysis questionable[2]

[1] Sample GD4 of Polenz and others (2018). Reported age is a concordia age for the youngest three zircons (of 100 analyzed). The youngest zircon at this site yielded a 38 ±2 Ma age.

[2] Detrital zircon analysis on siltstone. Four Pliocene and Miocene zircons in this sample from the Lincoln Creek Formation type section indicate sample contamination; results from all zircons in this sample are therefore questionable. Complete analytical data are in the Rochester quadrangle Data Supplement.